DOI: 10.26599/FSHW.2026.9251172

Contents lists available at SciOpen

Food Science and Human Wellness

journal homepage: https://www.sciopen.com/journal/2097-0765

China Food Publishing Co.

Polystyrene Nanoplastics Chronic Exposure Aggravates Diabetic Kidney Injury in mice: role of mtROS/Sirt1 axis mediated renal tubular senescence

Xialei Liu[1], Jie Dai[1], Peng Li[1], Tao Wu[1], Lan He[1], Yijun Dong[1], Jiamiao Qin[1], Lina Zhao[1,2]*

[1]*Department of Nutrition, School of Public Health, Wuhan University, Wuhan, Hubei, China*

[2]*NHC Specialty Laboratory of Food Safety Risk Assessment and Standard Development, Hubei, China*

ABSTRACT: Previous studies have suggested that polystyrene nanoplastics (PS-NPs) preferentially accumulate in the kidneys, posing a new threat to people with diabetic nephropathy. However, the adverse effect of chronic exposure of PS-NPs on diabetic kidney and underlying mechanisms remain largely unknown. Diabetic mice were orally administered PS-NPs (80 nm) at different doses (1, 10, and 50 mg/kg/day) for 60 days. PS-NPs was found mainly accumulated in the renal tubules rather than the glomeruli and caused tubular-specific damage as indicated by both pathological changes and increased levels of KIM-1/creatinine and NAG/creatinine in the urine. Mechanistically, the RNA-seq analysis of the kidney tissues of diabetic mice treated with PS-NPs revealed significant changes in mitochondrial-related genes. Co-localization of PS-NPs and mitochondria was detected in PS-NPs treated HK-2 cells, along with an increase in mtROS levels and a decrease in Sirt1 expression based on the experimental results from diabetic mice and HK-2 cells. Using the endocytosis inhibitor EIPA to inhibit the uptake of PS-NPs by HK-2 cells significantly reduced the mtROS levels within the cells. Furthermore, renal tubular senescence manifested by an increase in SA-β-galactosidase activity was further detected in both PS-NPs treated mice and HK-2 cells and that could be partially attenuated by the ROS inhibitor NAC. Overall, our study shows that PS-NPs mainly accumulate in the renal tubules rather than the glomeruli and can mediate the senescence of HK-2 cells by regulating the mtROS/Sirt1 axis.

Key words: Foodborne risk factor; Polystyrene Nanoplastics; Diabetic kidney; Renal tubular senescence; mtROS; Sirt1

1. Introduction

With the widespread application of plastic products in food packaging processes, the slow decomposition of plastics resulting in microplastics (MPs) and nanoplastics (NPs) has become an emerging foodborne risk factor[1].The average abundance of MPs detected in the 110 common solid foods and 36 common beverages was 639 items per kilogram[2]. The content of MPs in infant milk powder and milk bottles even reached 5 ± 3 per 100 grams and 65 ± 18 per liter[3]. Based on the average abundance of MPs in the takeout containers and the ordering frequency of high-risk groups (white-collar workers), the estimated weekly intake of MPs by people who order takeout 4-7 times a week was 12-203 pieces of MPs[4].

***Corresponding author**
zhaoln@whu.edu.cn

Received 25 July 2025
Received in revised from 22 October 2025
Accepted 29 January 2026

According to the standards of the European Union, MPs refer to plastic particles or fragments with a size less than 5 millimeters. MPs with a size less than 0.0001 millimeters are considered NPs[5]. Accumulating evidence indicates that[6] the fragmentation of plastic polymers does not stop at the micrometer level but further degrades and forms NPs, with the expected quantity being several orders of magnitude higher. Notably, due to their smaller particle size, NPs are more likely to pass through the intestinal barrier and enter the bloodstream, accumulating in organs and tissues over a long period of time[7]. Among the common types of plastic materials, polystyrene (PS) is an important thermoplastic. It is widely used in food and cosmetic packaging, and thus is more likely to be mixed into food and absorbed by the human body. Studies show that[8] the order of the amount of Micro-nano plastics (MNPs) released by heat treatment is as follows: PS > polypropylene > polyethylene terephthalate > polylactic acid. The health impacts of chronic exposure to PS-NPs at dietary-relevant concentrations are attracting great attention.

Diabetic nephropathy (DN) has become the leading cause of end-stage renal disease (ESRD) worldwide[9]. Approximately 50% of patients with Type 2 diabetes mellitus (T2DM) and 33.3% of patients with Type 1 diabetes mellitus (T1DM) will progress to DN[10]. Foodborne risk factors such as heavy metals, endocrine disruptors, and food additives have been shown to exert harmful effects on the kidney and aggravate DN[11, 12]. Accumulating evidence suggests that kidneys serve as the main organ for the accumulation and excretion of NPs[13, 14]. Studies have shown that[15, 16] the intestinal barrier of diabetic patients is damaged, and the risk of NPs accumulating in the body through the intestinal barrier increases. Therefore, compared to the general population, exposure to NPs in the diet may pose a greater threat to people with diabetes, and it may even increase the risk of DN for diabetic patients. However, the detrimental effect of chronic exposure to PS-NPs on the kidney under diabetic states has not been clearly investigated.

Previous studies have already detected MPs in the renal tubular epithelial cells of mice[17]. Considering that the upper limit size of the glomerular filtration barrier (GFB) is 10 nanometers[18], the degree of damage to the glomeruli and renal tubules may not be the same due to the excretion of NPs. The characteristics of kidney damage after chronic exposure to NPs need to be further deciphered. Recent studies have also reported that NPs can be taken up by multiple types of cells such as SH-SY5Y cells and intestinal epithelial cells, accumulating in the mitochondria and causing mitochondrial swelling and changes in membrane potential[19, 20]. Mitochondria are one of the main organelles responsible for reactive oxygen species (ROS) generation in cells which are intimately linked to the cell function and fate[21]. Disturbed ROS triggered premature senescence of endothelial cells and spermatogenic cells after chronic exposure to PS-NPs has been recently reported[22, 23]. The distribution of PS-NPs in the kidney, the most susceptible cell types, and whether PS-NPs exposure could result in kidney cell senescence, thereby inducing kidney damage, are largely unknown.

In this study, we hypothesized that mitochondrial reactive oxygen species (mtROS)-mediated cell senescence is critical to the renal tubular injury in diabetic mice exacerbated by PS-NPs exposure. First, histopathological and functional changes of kidney were detected in the diabetic mouse model orally

administered PS-NPs. Then, fluorescent-labeled PS-NPs were used to trace the location of NPs in the kidney of diabetic mouse model and track their distribution in the HK-2 cell according to transcriptomics findings. Lastly, the key role of mtROS/Sirt1 axis in mediating renal tubular injury induced by exposure to PS-NPs was further revealed using biomolecular techniques.

2. Materials and methods

2.1 Materials

Ethylisopropylamilorde (EIPA) was purchased from Ye Yuan (Shanghai, China). N-acetyl-L-cysteine (NAC) was obtained from Aladdin (Shanghai, China). The PS-NPs with a size of 80 nm and a concentration of 2.5% w/v, as well as the red fluorescent labeled PS-NPs with a size of 80 nm and a concentration of 1% w/v, were purchased from BaseLine Chromtech Research Centre (Tianjin, China). The in-depth characterization of PS-NPs is shown in Fig.S1. The β-actin rabbit monoclonal antibody (HA722023) was purchased from Huabio (Hangzhou, China), the Sirt1 rabbit monoclonal antibody (bs-0921R) and horseradish peroxidase-labeled goat anti-rabbit IgG (H+L) (bs-0295G-HRP) were purchased from Bioss (Beijing, China). The mouse frozen section ROS detection kit (HR9069) was purchased from Baiao Leibo (Beijing, China). Mitochondrial Superoxide Assay Kit (MitoSOX Red) (S0061S) was purchased from Beyotime (Shanghai, China). DAPI staining solution and Hoechst 33342 were purchased from Thermo (Shanghai, China) and Yeasen (Shanghai, China), respectively.

2.2 Animals and treatments

Eight-week-old male C57BL/6 mice were purchased from Vital River (Beijing, China). Under the standard 12-hour light-dark cycle pattern, the mice were raised in an indoor environment with controlled temperature (22 ± 2°C) and humidity (50-60%). Unlimited food and water were provided to the mice, and they were raised in a sterile environment free of pathogens. A diabetic mouse model was established through a four-week high-fat diet followed by intraperitoneal injection of streptozotocin (STZ; 50 mg/kg/day for three consecutive days). Diabetes was confirmed by measuring random blood glucose (RBG), and an RBG level ≥ 11.1 mM on two consecutive measurements was considered indicative of successful model establishment[24, 25] (Fig.S2). It is estimated that the daily intake for humans (~60 kg) is approximately 0.04-11.7 mg/kg. Based on body surface area and using the dose factor method for conversion from human to mouse doses, the equivalent dose for mice is approximately 0.5-144 mg/kg[26]. We selected the intervention doses for mice within the environmental-related concentration range as follows: 1, 10 and 50 mg/kg/day. The mice were randomly divided into the control group (Con group), the diabetic model group (DM group), the 1 mg/kg/day NPs intervention group (DM+1 NPs group), the 10 mg/kg/day NPs intervention group (DM+10 NPs group), and the 50 mg/kg/day NPs intervention group (DM+50 NPs group). The mice were given oral gavage every day between 9 a.m. and 12 p.m. for 60 days. All animal procedures strictly followed the guidelines of the Animal Ethics Committee of Wuhan University (WP20240356).

2.3 The accumulation and distribution of PS-NPs in the kidneys of mice

The detection of NPs tissue enrichment based on fluorescence signals refers to the research conducted by Xu et al.[14]. Preliminary experiments have confirmed that the fluorescent dyes do not leach out from the PS-NPs. The tissues were carefully arranged on trays and positioned on the platform of the *in vivo* imaging instrument (IVIS® Lumina Series III, PerkinElmer, MA, United States). The content of PS-NPs in the renal tissues was determined using the Cy5.5 channel in fluorescence mode. In addition, semi-quantitative analysis of the fluorescence of renal tissue was conducted using the Living Image software (PerkinElmer, MA, United States). The kidneys fixed in 4% formalin solution were extracted, embedded in paraffin, sectioned, stained with DAPI, and scanned using a single-color fluorescence scanner in the Cy5.5 channel to observe the distribution of PS-NPs in the kidney tissue.

2.4 Biochemical analysis

The urine of the mice was collected one day before the end of the experiment. In this study, the commercially available Kidney Injury Molecule 1 (KIM-1) and β-N-Acetylglucosaminidase (NAG) kits (Elabscience, Wuhan, China) were used to detect KIM-1 and NAG in urine. The biochemical kits (Elabscience, Wuhan, China) were used to measure the urine creatinine (Ucr), urine urea nitrogen (UUN) and microalbumin (Fig.S3) in the urine of mice. We followed the instructions provided by each kit for the processing. Specifically, the Ucr determination used the creatine oxidase method, and the UUN detection employed the urease method. All experimental procedures were carried out strictly in accordance with the manufacturer's guidelines.

2.5 Histopathological evaluation

The kidney tissue was fixed with a 4% paraformaldehyde solution. Then the tissue was dried, embedded in paraffin, and finally cut into 4 μm thick sections. The sections were stained using the hematoxylin-eosin (H&E) and Masson's trichrome (Masson) procedures. After the mounting medium solidified, the sections were scanned using a Nikon imaging system (Nikon, Tokyo, Japan). The morphological changes of renal tissue were observed using the Nikon Eclipse E100 optical microscope, and histopathological analysis was conducted. The degree of renal tubular injury was evaluated by observing 10 fields of view for each slice. The glomeruli and renal tubules were examined under a magnification of 40 times. The degree of renal tubular injury was evaluated by calculating the ratio of dilated/flat area of renal tubules, loss of brush border, formation of renal tubular cysts, renal tubular atrophy and vacuolation, and scoring was conducted[27]. The summary of the scoring system is as follows: 0 = not present, 1 = ≤ 10%, 2 = 11-25%, 3 = 26-45%, 4 = 46-75%, 5 = ≥ 76%. The degree of renal tubulointerstitial fibrosis was evaluated using Masson staining. This was achieved by dividing the area of collagen by the total area and then multiplying the result by 100.

2.6 RNA sequencing analysis

Transcriptome analysis was conducted by extracting RNA from kidney samples (3 mice in each group) and performing transcriptome sequencing on the Illumina platform. Principal component analysis (PCA) was used to visualize the gene expression profiles of different groups. The differential expression sequencing analysis (DESeq) method was used to conduct differential analysis of gene expression. The selection criteria for differentially expressed genes were the fold change in expression $|\log_2\text{FoldChange}| > 1$, and the significance P-value < 0.05, in order to identify the differentially expressed genes (DEGs). To identify the most significantly altered genes, a more stringent threshold was applied: $|\log_2\text{FoldChange}| > 5$ and P-value < 0.05.

2.7 Cell culture and treatment

The human proximal tubular epithelial cells (HK-2) were cultured in Dulbecco's Modified Eagle Medium (DMEM) containing 10% FBS and were maintained at 37℃ with 5% CO_2. The culture medium was replaced every two days. To establish a hyperglycemic model, cells were stimulated with 25 mM high glucose[28]. Based on the results of the cell viability experiment (Fig.S4A), HK-2 cells were exposed to different concentrations (1, 10, and 50 μg/mL) of PS-NPs in a high-glucose environment for 24 hours. To investigate the involvement of mtROS in this process, HK-2 cells were pretreated with either 10 μg/mL EIPA or 5 mM NAC before PS-NPs treatment.

2.8 Cellular internalization and distribution of PS-NPs

After being cultured and pre-treated as described above, the cells were stimulated with high glucose and then treated with 80 nm red fluorescent PS-NPs at concentrations of 1, 10, and 50 μg/mL for 24 hours. The cells were washed 3 times with serum-free medium and then stained with 100 nM MitoTracker Green (Servicebio, Wuhan, China) for 30 minutes. Finally, they were washed 2-3 times with serum-free medium to remove the unbound probe. After fixation and permeabilization, the cell nucleus was stained blue for 10 minutes using 0.2 μg/mL DAPI staining solution. The co-localization of fluorescent PS-NPs with mitochondria and cell nucleus was captured under a fluorescence microscope.

2.9 Mitochondrial membrane potential detection

Cells were cultured and treated as described in the previous section. After adding the mitochondrial membrane potential fluorescent probe JC-1 (Elabscience, Wuhan, China) to the wells, the cells were incubated at 37°C in the dark for 20 minutes, washed twice, and observed under a fluorescence microscope to assess the changes in mitochondrial membrane potential.

2.10 ROS detection

According to the instructions of the Mouse Tissue Slice ROS Detection Kit and Mitochondria Superoxide Assay Kit, DHE probe and MitoROS probe were used to detect the ROS levels in mouse kidney tissue and HK-2 cell mitochondria, respectively. DAPI staining solution and Hoechst 33342 were employed for nuclear staining of mouse kidney tissue and HK-2 cells, respectively. The samples were observed under a fluorescence microscope, and quantitative analysis was performed using ImageJ software.

2.11 Senescence-associated β-galactosidase (SA-β-gal) staining

The SA-β-gal staining procedure was carried out according to the protocol provided by the commercial staining kit from Beyotime Biotechnology (Shanghai, China). The senescence of kidney tissues and HK-2 cells was examined, and images of the cells stained with the dye were captured using a microscope for observation[29].

2.12 Quantitative real-time polymerase chain reaction (qRT-PCR)

Total RNA was extracted using TRIeasy reagent (Yeasen, Shanghai, China) in accordance with the instructions provided by the manufacturer. cDNA was synthesized using the reverse transcription kit (Vazyme, Nanjing, China). For the qRT-PCR analysis, the qPCR kit (Vazyme, Nanjing, China) was used. The quantitative method ($2^{-\Delta\Delta Ct}$) was employed to calculate and process the results of the target gene. *β-actin* (the housekeeping gene) was used for normalization. The primer sequences for *P21*, *P53*, *Rb*, *β-actin*, and *Sirt1* were supplied by Shanghai Bioengineering Corporation (Shanghai, China). The primer sequences used were as follows: p21: forward(F)-ctgtcttgtacccttgtgcctc, reverse(R)-tggagtggtagaaatctgtcatgct; p53: F-acctatggaaactacttcctgaaa, R-tccggggacagcatcaaatc; Rb: F-acttctactcgaacacgaatgc, R-cagtgtccaccaaggtcctg; β-actin: F-gagaaaatctggcaccacacc, R-ggatagcacagcctggatagcaa; Sirt1: F-tcctggacaattccagccat, R-tttggattcccgcaacctgt.

2.13 Western blot

The kidney tissue was lysed using the radioimmunoprecipitation assay (RIPA) lysis buffer, which was supplemented with 1% (w/v) phenylmethylsulfonyl fluoride (PMSF) as a protease inhibitor (Epizyme Biotech, Shanghai, China). The protein concentration was determined using the BCA protein assay kit (Elabscience, Wuhan, China). Equal amounts of protein were mixed with SDS loading buffer and subjected to electrophoresis. The proteins were then transferred onto a PVDF membrane, which was subsequently incubated with the designated primary antibody at 4°C overnight, followed by incubation with the corresponding secondary antibody at room temperature for 1 hour. The proteins on the membrane were detected using the electrochemiluminescence (ECL) method. Finally, the intensity of the target protein bands was measured using the ImageJ software. The HK-2 cells under a high-glucose environment were treated with PS-NPs, then washed with PBS. They were lysed in the lysis buffer for 30 minutes, and the subsequent western blotting steps were identical to those described for kidney tissues.

2.14 Statistical analysis

Statistical analysis was performed using GraphPad Prism software (GraphPad Software Inc, San Diego, CA, USA). Data were presented as mean ± SEM. The differences among the groups were evaluated using one-way analysis of variance (ANOVA), and then multiple comparisons were conducted using the Dunnett test. The concept of statistical significance was achieved by setting the threshold for *P*-value to be less than 0.05.

3. Results

3.1 PS-NPs accumulate in renal tubules and cause specific damage

Biofluorescence imaging analysis revealed that PS-NPs accumulated significantly in the kidneys of diabetic mice treated with PS-NPs at dosage (Fig.1A). Compared with the fluorescence signal intensity of the kidneys in the diabetic model group, there was a statistically significant difference in the fluorescence intensity of the kidneys in the highest-dose intervention group (Fig.1B). The results of DAPI staining and single-color fluorescence scanning further confirmed that PS-NPs mainly accumulated in the renal tubules rather than the glomeruli in the kidneys (Fig.1C).

KIM-1 and NAG are regarded as sensitive indicators for renal tubular damage[30-32]. By detecting KIM-1 and NAG in the urine of mice and correcting with urine creatinine, it was found that the levels of KIM-1/creatinine and NAG/creatinine in the urine of the mice in the highest-dose intervention group were significantly increased (Fig.1D,E), confirming that the accumulation of PS-NPs in the renal tubules of diabetic mice caused renal tubular-specific damage.

In summary, the above results clearly indicate that PS-NPs mainly accumulate in the renal tubules, leading to specific functional damage in the renal tubules.

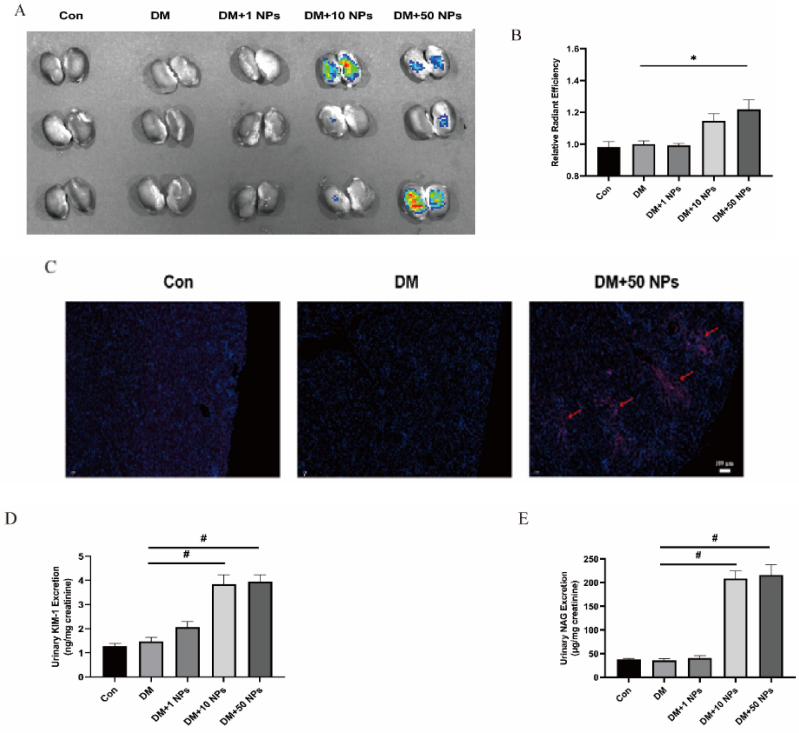

Fig.1 PS-NPs accumulate in renal tubules and cause specific damage. (A) Accumulation of PS-NPs in the kidneys of diabetic mice. (B) Semi-quantitative analysis of fluorescence intensity. (C) Distribution of PS-NPs in the kidneys of diabetic mice (100 x). Scale bar = 100 μm. (D, E) The levels of KIM-1/creatinine and NAG/creatinine in the urine of mice. (n≥6 per group). $^{*}P < 0.05$, $^{\#}P < 0.001$.

3.2 PS-NPs mediate tubular pathological injury and fibrosis via the induction of tubular cell senescence

Pathological changes in kidney tissue were observed by H&E and Masson staining. Compared with the DM group, the PS-NPs intervention groups exhibited renal tubular injury characterized by vacuolar degeneration of epithelial cells, tubular atrophy, reduced tubular volume, and narrowed lumens. These pathological changes were more pronounced in the DM+50 NPs group (Fig.2A). The renal tubule scores

also showed that compared with the DM group, the renal tubular damage in the DM+50 NPs group was significantly more severe (Fig.2B). The results of Masson staining further confirmed these changes. In diabetic mice exposed to PS-NPs, the blue color of the renal tubular collagen fibers was significantly enhanced (Fig.2C, D), indicating increased deposition of these fibers induced by PS-NPs.

To further investigate the mechanism of PS-NP-induced renal tubular injury in diabetic mice, we assessed the activity of SA-β-gal, a key marker of cellular senescence[33] in renal tissue sections. We observed that SA-β-gal activity was elevated in the PS-NP-treated groups. Notably, the highest-dose group (DM+50 NPs) exhibited the most significant increase in enzymatic activity (Fig.2E, F). The staining results of SA-β-gal activity in HK-2 cells after PS-NPs intervention also confirmed these findings (Fig.2G, H).

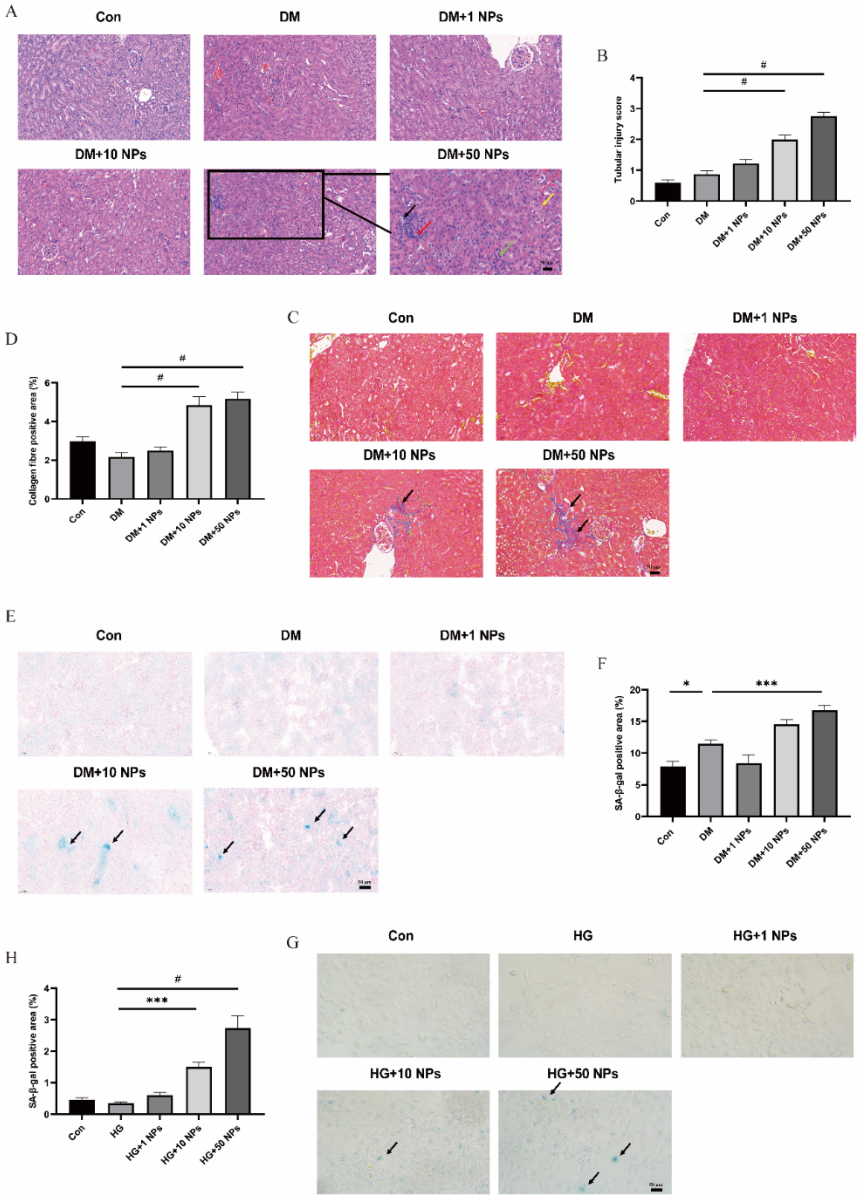

Fig.2 PS-NPs mediate tubular pathological injury and fibrosis via the induction of tubular cell senescence. (A) Representative image of H&E staining of kidney tissue (200 x). Scale bar = 50 μm. Light green arrow, narrowing of renal capsule; Yellow arrow, vacuolar degeneration of renal tubular epithelial cells; Black arrow, atrophy of renal tubules; Red arrow, infiltration of lymphocytes. (B) Renal tubule injury score. (C) Representative image of Masson staining of renal tissue (200 x). Scale bar = 50 μm. (D) Proportion of Masson-positive area. (E) Representative images of SA-β-gal staining of renal sections from each group (200 x). Scale bar = 50 μm. (F) Semi-quantitative analysis of renal SA-β-gal staining. (G) Representative images of SA-β-gal staining of HK-2 cells in each group (200 x). Scale bar = 50 μm. (H) Semi-quantitative analysis of SA-β-gal staining in HK-2 cells. (n≥3 per group). $^{*}P < 0.05$, $^{***}P < 0.005$, $^{\#}P < 0.001$.

3.3 Mitochondria are revealed as the accumulation site of PS-NPs by transcriptomic assay and in HK-2 cells

Based on transcriptome data, we conducted differential analysis of gene expression using the DESeq software package in R language to explore the underlying mechanism of renal tubular senescence. The conditions for screening differentially expressed genes were the fold change in expression $|\log_2\text{FoldChange}| > 1$, and the significance P-value < 0.05. By comparing the gene expressions of the DM+50 NPs group with those of the DM group, a total of 689 differentially expressed genes were identified (Fig.3A). We selected 22 genes with the most significant differences through expression fold changes $|\log_2\text{FoldChange}| > 5$ and significant P-value < 0.05 (Fig.3B). There are two genes that are clearly related to organelle function, namely Ucp1 and Cox8b, and both exhibit a strong connection with mitochondrial function[34] (Fig.3C). This suggests that PS-NPs may induce cellular senescence by accumulating in mitochondria and perturbing their function.

To further validate the cellular location of PS-NPs, HK-2 cells were treated with fluorescent PS-NPs. It was found that the uptake of PS-NPs by HK-2 cells was dose-dependent under high glucose stimulation (Fig.3D, E). Mitochondria and nuclei were stained green and blue, respectively, for co-localization with the red fluorescent PS-NPs. Previous studies have shown that red fluorescence and green fluorescence overlap to form orange[35]. In Fig.3F, the red fluorescence of PS-NPs overlaps with the green fluorescence of mitochondria, resulting in an orange color. The results demonstrate that PS-NPs are primarily localized to mitochondria. In addition, some diffuse red signals were also observed in the cytoplasm, which may represent PS-NPs distributed in other cytoplasmic organelles.

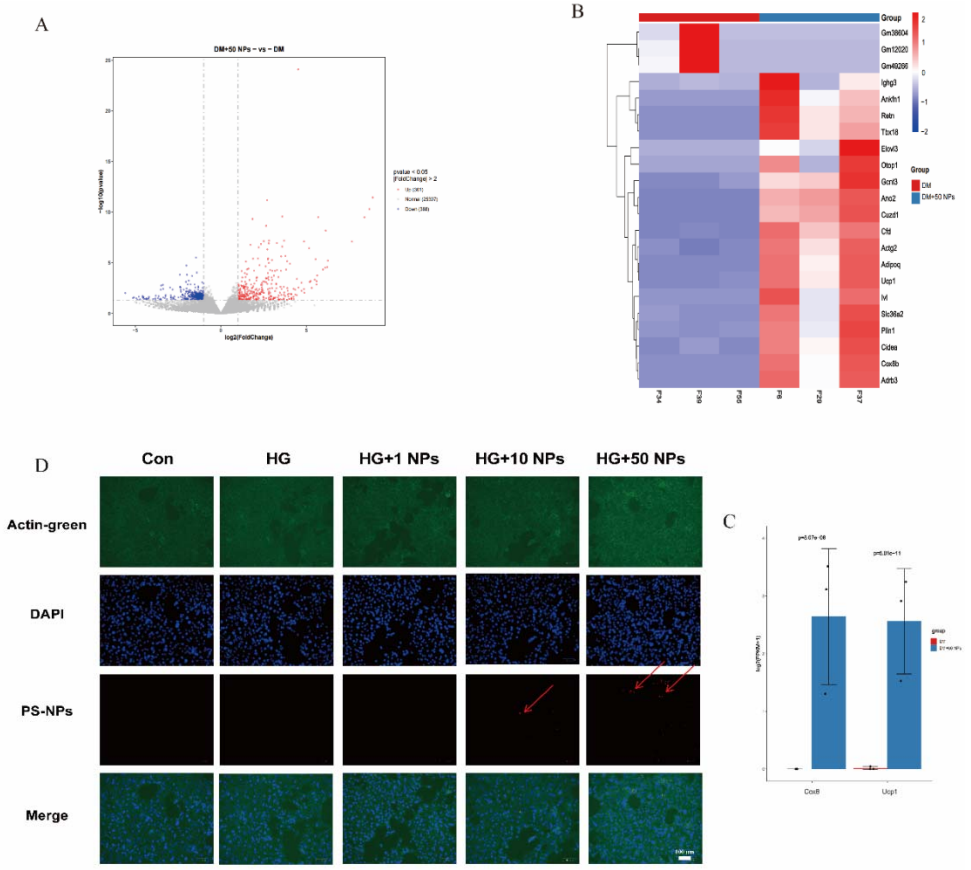

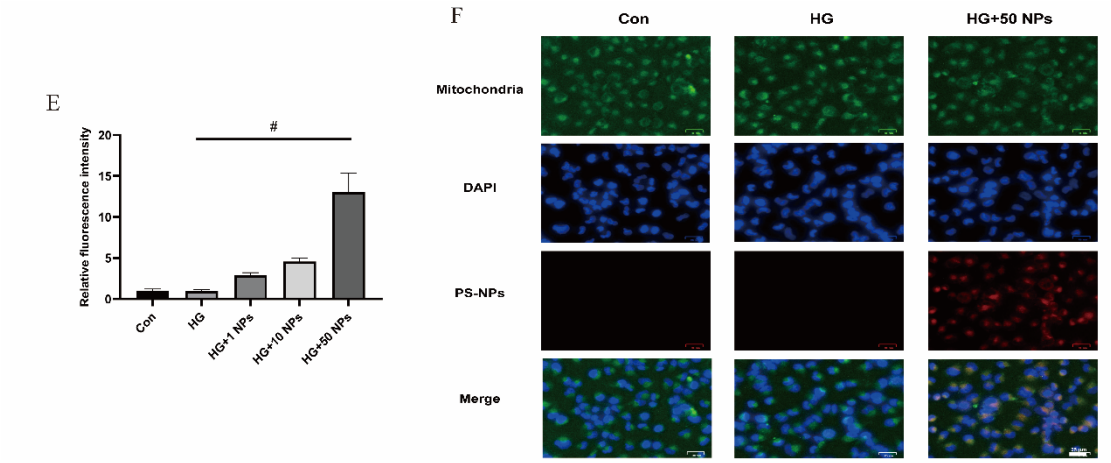

Fig.3 Mitochondria are revealed as the accumulation site of PS-NPs by transcriptomic assay and in HK-2 cells. (A) Volcanic plot displaying differentially expressed genes in the kidneys between the DM+50 NPs and DM groups. (B) The heat map of the genes with the most significant difference. Each column represents data from a single mouse. The color intensity represents the Z-score. (C) Significant changes in mitochondrial function related genes. (D) Representative images showing PS-NP uptake (100 x). Scale bar = 100 μm. Actin-green represents the view of the cell skeleton, DAPI represents the view of the cell nucleus, PS-NPs represents the view of the fluorescent NPs and merge represents the combined view. (E) Quantitative results of the uptake of HK-2 cells by PS-NPs. (F) Distribution of PS-NPs in HK-2 cells (400 x). Scale bar = 25 μm. The Con group represents the control group using the ordinary culture medium, the HG group represents the model group using the high-glucose culture medium, the HG+1 NPs group represents the intervention group with 1 μg/mL PS-NPs, the HG+10 NPs group represents the intervention group with 10 μg/mL PS-NPs and the HG+50 NPs group represents the intervention group with 50 μg/mL PS-NPs. (n≥3 per group). $^{\#}P < 0.001$.

3.4 PS-NPs induce changes in mitochondrial membrane potential and increase ROS levels both in vitro and in vivo

The mitochondrion is a major site for maintaining redox homeostasis between ROS generation and scavenging[36]. We evaluated the mitochondrial membrane potential and mtROS levels of HK-2 cells exposed to high glucose stimulation after being in contact with different concentrations of PS-NPs. The results showed that exposure to PS-NPs led to depolarization of the mitochondrial membrane potential and an increase in mtROS levels in HK-2 cells (Fig.4A-D). To further investigate the biological effects of PS-NPs on renal tubules, we measured the ROS levels in renal tissue sections of diabetic mice. As shown in Fig.4E, F, compared with the kidneys of the DM group, the ROS levels in the kidneys of the DM+50 NPs group were significantly higher. Combined *in vivo* and *in vitro* ROS measurements demonstrated that PS-NPs exposure significantly elevated ROS levels in renal tubules, an effect predominantly attributed to a surge in mtROS. It is plausible that the elevation in mtROS mediates the renal tubular senescence triggered by PS-NPs.

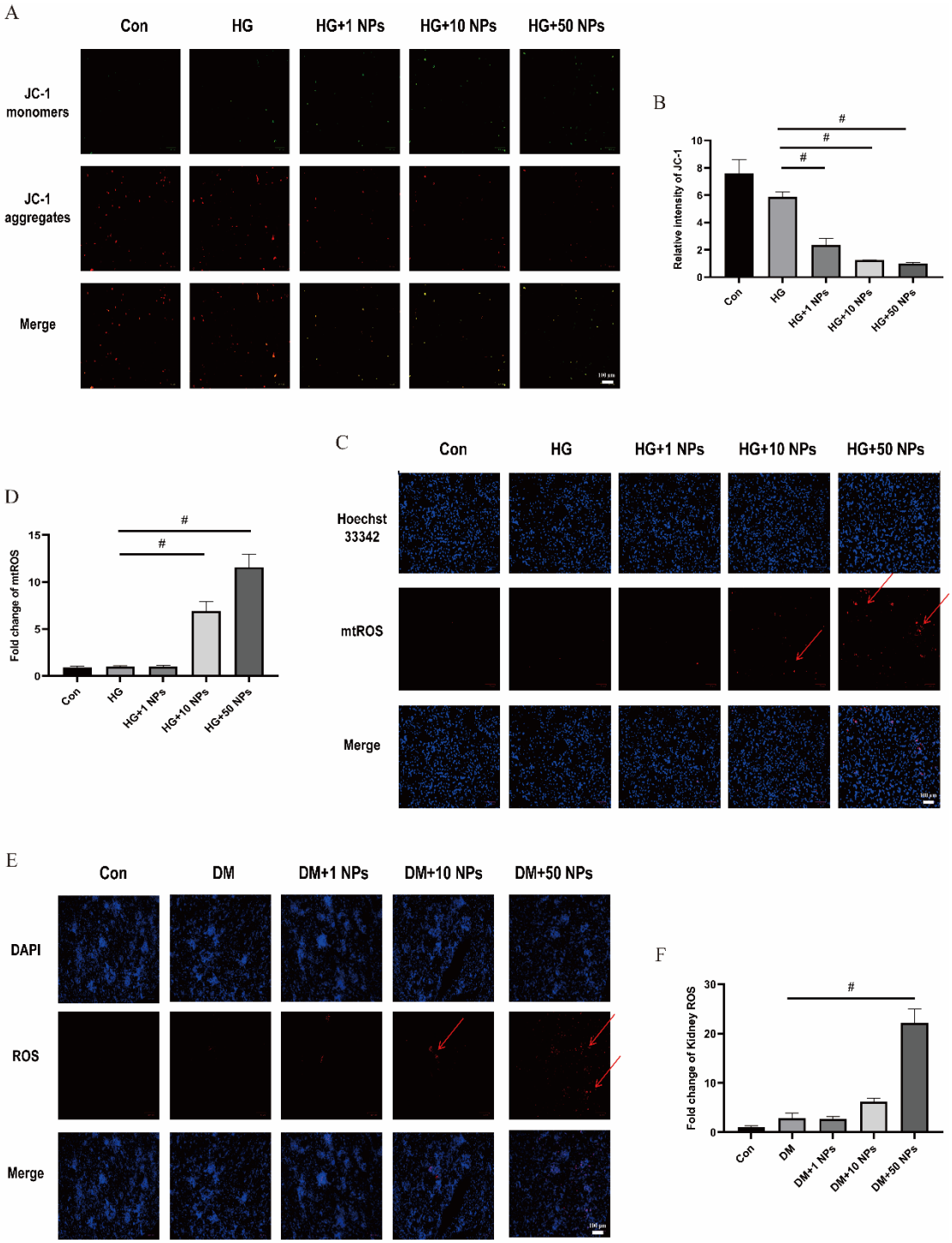

Fig.4 PS-NPs induce changes in mitochondrial membrane potential and increase ROS levels both *in vitro* and *in vivo*. (A) Assessment of mitochondrial membrane potential in HK-2 cells using JC-1 staining (100 x). Scale bar = 100 μm. (B) Semi-quantitative analysis of mitochondrial membrane potential changes. (C) Detection of mtROS in HK-2 cells (100 x). Scale bar = 100 μm. (D) Semi-quantitative analysis of mtROS generation levels in HK-2 cells. (E) Detection of ROS in the kidneys (100 x). Scale bar = 100 μm. (F) Semi-quantitative analysis of ROS production levels in the kidneys. (n≥3 per group). $^{\#}P < 0.001$.

3.5 PS-NPs induce senescence in renal tissue and HK-2 cells by targeting the anti-senescence gene Sirt1

The activation of the p53/p21 and Rb/p16 signaling pathways is a key molecular event marking the beginning of cellular senescence[37]. Previous studies have shown that Sirt1 is a member of the NAD^+-dependent deacetylase family[38], which can inhibit cellular senescence by maintaining mitochondrial antioxidant function[39]. In this study, it was also observed that the mRNA expression levels of *P53*, *P21*, and

Rb increased, while the mRNA expression level of *Sirt1* decreased in the HK-2 cells treated with PS-NPs (Fig.5A). Consistent with the changes in mRNA expression levels, the protein expression level of Sirt1 was found to be decreased after PS-NPs intervention both *in vivo* (Fig.5B, C) and *in vitro* (Fig.6C, D). These results suggest that PS-NPs exposure induces renal tubular senescence, with the anti-senescence gene Sirt1 implicated as a potential mediator.

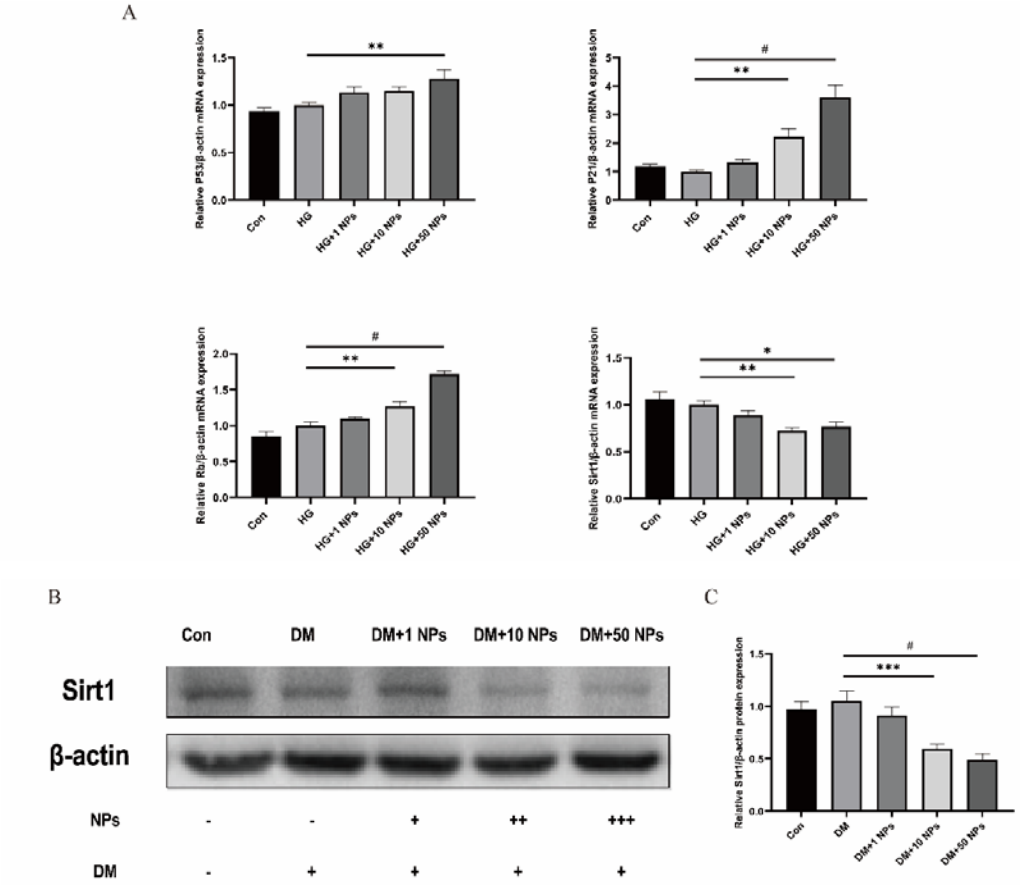

Fig.5 PS-NPs induce senescence in renal tissue and HK-2 cells by targeting the anti-senescence gene Sirt1. (A) Relative expression levels of *P53*, *P21*, *Rb* and *Sirt1* mRNA *in vitro*. (B) Representative images of western blot analysis *in vivo*. (C) Quantification of western blot band intensity *in vivo.* (n ≥ 3 per group). $^{*}P < 0.05$, $^{**}P < 0.01$, $^{***}P < 0.005$, $^{\#}P < 0.001$.

3.6 The mtROS/Sirt1 axis plays a pivotal role in the underlying mechanism of PS-NP-induced cellular senescence in HK-2 cells

Based on the known role of ROS in inducing senescence[40], we propose that PS-NPs induce HK-2 cell senescence through the mtROS/Sirt1 pathway. In order to further verify that the mtROS/Sirt1 axis plays a crucial role in the acceleration of HK-2 cell senescence by PS-NPs, we employed the endocytosis inhibitor EIPA and the antioxidant NAC in HG-stimulated HK-2 cells treated with PS-NPs. Based on CCK-8 viability assays (Fig.S4B, C), we employed non-cytotoxic concentrations of EIPA and NAC, which alone exerted no detectable toxicity on HK-2 cells. The suppression of intracellular endocytosis by EIPA significantly blunted mtROS generation in high glucose-stimulated HK-2 cells (Fig.6A, B). The expression level of Sirt1 protein after NAC intervention is shown in Fig.6C. Compared with the HG+50 NPs group, the expression level of Sirt1 protein in the NAC intervention group was significantly increased (Fig.6D), while SA-β-gal enzyme

activity was significantly inhibited (Fig.6E, F). The above results confirm that the mtROS/Sirt1 axis plays a crucial role in the exacerbation of diabetic renal tubular senescence by PS-NPs.

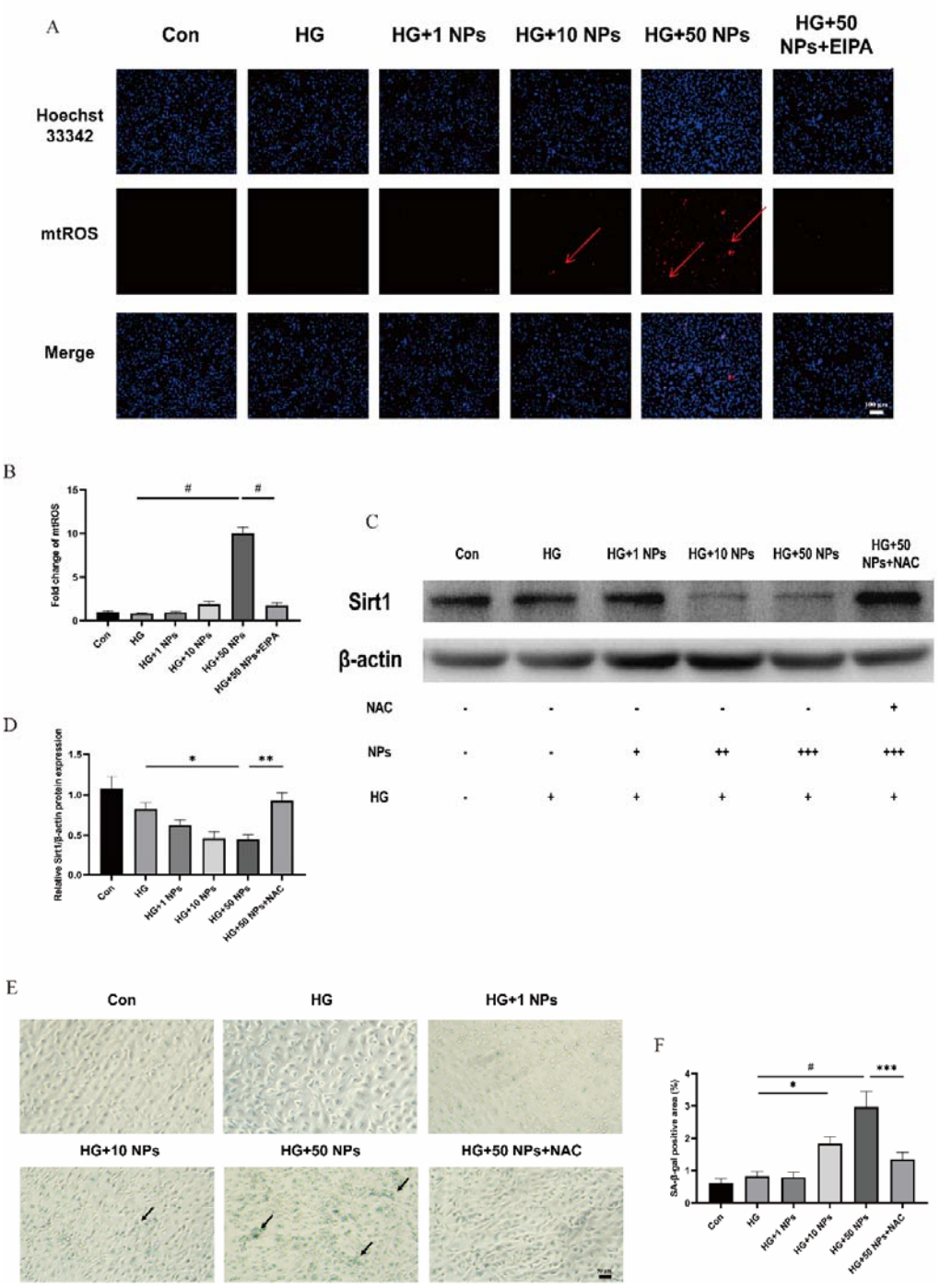

Fig.6 The mtROS/Sirt1 axis plays a pivotal role in the underlying mechanism of PS-NP-induced cellular senescence in HK-2 cells. (A) The generation of mtROS after EIPA intervention in HK-2 cells (100 x). Scale bar = 100 μm. (B) Semi-quantitative analysis of mtROS generation levels after EIPA intervention in HK-2 cells. (C) Representative image of western blot *in vitro*. (D) Quantification of western blot band intensity *in vitro*. (E) Representative images of SA-β-gal staining between groups after NAC intervention in HK-2 cells (200 x). Scale bar = 50 μm. (F) Semi-quantitative analysis of SA-β-gal staining after NAC intervention in HK-2 cells. (n≥3 per group). $^{*}P < 0.05$, $^{**}P < 0.01$, $^{***}P < 0.005$, $^{\#}P < 0.001$.

4. Discussion

In this study, we established a diabetic mouse model. Previous literature and internal functional markers verification have shown that compared with normal mice, the diabetic mice alone did not show significant kidney damage[9]. Our study confirms that PS-NPs are mainly distributed in the renal tubules of

the kidney, causing specific damage to the tubules. Through transcriptomic analysis and organelle localization, it was found that PS-NPs were mainly distributed in mitochondria and caused an increase in mtROS after internalization by cells. This evidence further confirms that the mtROS/Sirt1 axis constitutes a key mechanism whereby PS-NPs exacerbate high glucose-induced senescence in HK-2 cells. This study is significant in elucidating the detrimental effects of chronic oral exposure to PS-NPs on the kidneys of diabetic mice.

Previous studies have confirmed that MNPs can accumulate in the kidneys[17]. How MNPs distribute within the kidney and inflict cell-specific damage is not yet fully understood. Through fluorescence co-localization, for the first time we confirmed that the renal tubules are the main accumulation site of NPs in the kidneys and the specific indicators of renal tubule damage, KIM-1 and NAG, were used to confirm the specific damage of renal tubules. Regarding the reasons for the differences in the distribution of nano-plastics in the kidneys, based on previous research reports, we hypothesized that 80nm PS NPs cannot pass through the glomerular filtration barrier and accumulate in the glomeruli. Instead, they are absorbed by the epithelial cells of the proximal tubules and excreted into the renal tubular lumen through the renal tubular secretion system, and then expelled through urine[41]. Therefore, PS-NPs mainly accumulate in the renal tubules rather than the glomeruli. The study results further confirm that during the excretion process of nano-plastics, the damage to the renal tubules may be much greater than that to the glomeruli.

The differentially expressed genes identified through transcriptomics analysis of kidney tissue, namely Ucp1[42] and Cox8b[43], are closely related to mitochondrial function. We used fluorescence co-localization to track the subcellular localization of PS-NPs in HK-2 cells, which confirmed that PS-NPs were mainly distributed in mitochondria after being taken up by HK-2 cells, resulting in depolarization of the mitochondrial membrane potential and an increase in mtROS levels. Consistent with our research results, a recent study of renal injury induced by inhalation exposure to airborne NPs also observed the presence of NPs in the mitochondria of HK-2 cells[5], which led to depolarization of the mitochondrial membrane potential and an increase in the total ROS level within the cells. Building on this finding, we conducted further exploration and ultimately confirmed that mitochondria are the main organelle for the distribution of PS-NPs and the increase in mtROS levels.

Multiple studies have shown that ROS is an important inducer of senescence[40]. Previous studies have confirmed that NPs can cause senescence in various cells, including cardiomyocytes[44], skeletal muscle progenitor cells[45], esophageal epithelial cells[46], gastric epithelial cells[47], and bone marrow hematopoietic cells[48], most of which were mediated by oxidative stress. The study by Lu[49] confirmed that NPs induce oxidative stress in pig kidney cells, leading to the accumulation of ROS in mitochondria and ultimately triggering the senescence of kidney cells, providing new evidence for the nephrotoxicity of NPs. These results suggest that cellular senescence mediated by mtROS is a key pathogenic mechanism underlying PS-NP-induced renal tubular injury. Stress induced senescence of renal tubular cells is an early pathological change[50]. This phenotype is characterized by the upregulation of KIM-1[51], as confirmed by our data.

Several *in vivo* and *in vitro* experiments have shown that renal tubular cell senescence plays an important role in DN progression[52-54], and activation of anti-senescence gene Sirt1 can alleviate renal interstitial damage in diabetes[55]. In this study, the enhanced SA-β-gal activity *in vitro* and *in vivo*, as well as the increased mRNA expression levels of senescence signaling molecules *P53*, *P21*, and *Rb*, suggest that PS-NPs may induce senescence of renal tubular cells. Our study demonstrates for the first time that PS-NP exposure mediates HK-2 cell senescence via the mtROS/Sirt1 axis. This finding provides a novel mechanistic insight into how PS-NPs exacerbate renal tubular injury in diabetes and suggests a potential target for the prevention and treatment of DN.

5. Conclusion

In conclusion, our study confirmed that PS-NPs exposure aggravated renal damage in diabetic mice in a dose-dependent manner, and the damage mechanism involves that PS-NPs were mainly distributed in renal tubules, causing specific damage to renal tubules. We further tracked the subcellular localization of PS-NPs after internalization by HK-2 cells and found that PS-NPs were mainly distributed in mitochondria, causing an increase in mtROS. Our study establishes the mtROS/Sirt1 axis as a key mechanism in PS-NP-induced renal tubular cell senescence. A limitation of this study is that although we have elucidated the molecular mechanism of PS-NP-induced renal tubular senescence, this pathway was not directly validated in our animal model. Future studies should also integrate population-based epidemiological evidence to quantify the disease burden and attributable risk of PS-NPs exposure in diabetic kidney injury, thereby clarifying the role of this foodborne risk factor in the progression of DN.

References

[1] H. Zha, S. Han, R. Tang, et al., Polylactic acid micro/nanoplastic-induced hepatotoxicity: Investigating food and air sources via multi-omics, Environ Sci Ecotechnol. 21 (2024) 100428. https://doi.org/10.1016/j.ese.2024.100428.

[2] C.L. Bai, L.Y. Liu, J.L. Guo, et al., Microplastics in take-out food: Are we over taking it?, Environ Res. 215 (2022) 114390. https://doi.org/10.1016/j.envres.2022.114390.

[3] Q. Zhang, L. Liu, Y. Jiang, et al., Microplastics in infant milk powder, Environ Pollut. 323 (2023) 121225. https://doi.org/10.1016/j.envpol.2023.121225.

[4] F. Du, H. Cai, Q. Zhang, et al., Microplastics in take-out food containers, J Hazard Mater. 399 (2020) 122969. https://doi.org/10.1016/j.jhazmat.2020.122969.

[5] L. Chen, B. Han, S. Yang, et al., Toxicological effects and mechanisms of renal injury induced by inhalation exposure to airborne nanoplastics, J Hazard Mater. 488 (2025) 137393. https://doi.org/10.1016/j.jhazmat.2025.137393.

[6] N. Qian, X. Gao, X. Lang, et al., Rapid single-particle chemical imaging of nanoplastics by SRS microscopy, Proc Natl Acad Sci U S A. 121 (2024) e2300582121. https://doi.org/10.1073/pnas.2300582121.

[7] L. Rubio, I. Barguilla, J. Domenech, et al., Biological effects, including oxidative stress and genotoxic damage, of polystyrene nanoparticles in different human hematopoietic cell lines, J Hazard Mater. 398 (2020) 122900. https://doi.org/10.1016/j.jhazmat.2020.122900.

[8] T. Jin, Y. Liu, H. Lyu, et al., Plastic takeaway food containers may cause human intestinal damage in routine life usage: Microplastics formation and cytotoxic effect, J Hazard Mater. 475 (2024) 134866. https://doi.org/10.1016/j.jhazmat.2024.134866.

[9] H.T. Cheng, X. Xu, P.S. Lim, et al., Worldwide Epidemiology of Diabetes-Related End-Stage Renal Disease, 2000-2015, Diabetes Care. 44 (2021) 89-97. https://doi.org/10.2337/dc20-1913.

[10] Y. Guo, Z. Ran, Y. Zhang, et al., Marein ameliorates diabetic nephropathy by inhibiting renal sodium glucose transporter 2 and activating the AMPK signaling pathway in db/db mice and high glucose-treated HK-2 cells, Biomed Pharmacother. 131 (2020) 110684. https://doi.org/10.1016/j.biopha.2020.110684.

[11] X. Li, X. Ye, L. Xu, et al., Association between endocrine disrupting chemicals exposure and diabetic kidney disease in adults: A national cross-sectional NHANES study, Ecotoxicol Environ Saf. 293 (2025) 118044. https://doi.org/10.1016/j.ecoenv.2025.118044.

[12] Y. Zhang, X. Gong, R. Li, et al., Exposure to cadmium and lead is associated with diabetic kidney disease in diabetic patients, Environ Health. 23 (2024) 1. https://doi.org/10.1186/s12940-023-01045-z.

[13] M.H. Lamoree, J. van Boxel, F. Nardella, et al., Health impacts of microplastic and nanoplastic exposure, Nat Med. 31 (2025) 2873-2887. https://doi.org/10.1038/s41591-025-03902-5.

[14] D. Xu, Y. Ma, X. Han, et al., Systematic toxicity evaluation of polystyrene nanoplastics on mice and molecular mechanism investigation about their internalization into Caco-2 cells, J Hazard Mater. 417 (2021) 126092. https://doi.org/10.1016/j.jhazmat.2021.126092.

[15] D. Arnone, C. Chabot, A.C. Heba, et al., Sugars and Gastrointestinal Health, Clin Gastroenterol Hepatol. 20 (2022) 1912-1924.e1917. https://doi.org/10.1016/j.cgh.2021.12.011.

[16] W.H. Hsu, Y.Z. Chen, Y.T. Chiang, et al., Polystyrene nanoplastics disrupt the intestinal microenvironment by altering bacteria-host interactions through extracellular vesicle-delivered microRNAs, Nat Commun. 16 (2025) 5026. https://doi.org/10.1038/s41467-025-59884-y.

[17] Y.L. Wang, Y.H. Lee, Y.H. Hsu, et al., The Kidney-Related Effects of Polystyrene Microplastics on Human Kidney Proximal Tubular Epithelial Cells HK-2 and Male C57BL/6 Mice, Environ Health Perspect. 129 (2021) 57003. https://doi.org/10.1289/ehp7612.

[18] J.E. Zuckerman, C.H. Choi, H. Han, et al., Polycation-siRNA nanoparticles can disassemble at the kidney glomerular basement membrane, Proc Natl Acad Sci U S A. 109 (2012) 3137-3142. https://doi.org/10.1073/pnas.1200718109.

[19] Y. Huang, B. Liang, Z. Li, et al., Polystyrene nanoplastic exposure induces excessive mitophagy by activating AMPK/ULK1 pathway in differentiated SH-SY5Y cells and dopaminergic neurons in vivo, Part Fibre Toxicol. 20 (2023) 44. https://doi.org/10.1186/s12989-023-00556-4.

[20] D. Xu, Y. Ma, C. Peng, et al., Differently surface-labeled polystyrene nanoplastics at an environmentally relevant concentration induced Crohn's ileitis-like features via triggering intestinal epithelial cell necroptosis, Environ Int. 176 (2023) 107968. https://doi.org/10.1016/j.envint.2023.107968.

[21] T.C. Wikramanayake, J. Chéret, A. Sevilla, et al., Targeting mitochondria in dermatological therapy: beyond oxidative damage and skin aging, Expert Opin Ther Targets. 26 (2022) 233-259. https://doi.org/10.1080/14728222.2022.2049756.

[22] Y. Liang, Y. Yang, C. Lu, et al., Polystyrene nanoplastics exposure triggers spermatogenic cell senescence via the Sirt1/ROS axis, Ecotoxicol Environ Saf. 279 (2024) 116461. https://doi.org/10.1016/j.ecoenv.2024.116461.

[23] S. Shiwakoti, J.Y. Ko, D. Gong, et al., Effects of polystyrene nanoplastics on endothelium senescence and its underlying mechanism, Environ Int. 164 (2022) 107248. https://doi.org/10.1016/j.envint.2022.107248.

[24] D.J. Borg, R. Wang, L. Murray, et al., The effect of interleukin-22 treatment on autoimmune diabetes in the NOD mouse, Diabetologia. 60 (2017) 2256-2261. https://doi.org/10.1007/s00125-017-4392-2.

[25] L. Li, P. Krznar, A. Erban, et al., Metabolomics Identifies a Biomarker Revealing In Vivo Loss of Functional β-Cell Mass Before Diabetes Onset, Diabetes. 68 (2019) 2272-2286. https://doi.org/10.2337/db19-0131.

[26] W. Xu, Y. Yuan, Y. Tian, et al., Oral exposure to polystyrene nanoplastics reduced male fertility and even caused male infertility by inducing testicular and sperm toxicities in mice, J Hazard Mater. 454 (2023) 131470. https://doi.org/10.1016/j.jhazmat.2023.131470.

[27] L. Feng, C. Chen, X. Xiong, et al., PS-MPs promotes the progression of inflammation and fibrosis in diabetic nephropathy through NLRP3/Caspase-1 and TGF-β1/Smad2/3 signaling pathways, Ecotoxicol Environ Saf. 273 (2024) 116102. https://doi.org/10.1016/j.ecoenv.2024.116102.

[28] C. Noonin, V. Thongboonkerd, Curcumin prevents high glucose-induced stimulatory effects of renal cell secretome on fibroblast activation via mitigating intracellular free radicals and TGF-β secretion, Biomed Pharmacother. 174 (2024) 116536. https://doi.org/10.1016/j.biopha.2024.116536.

[29] C. Pan, Y. Wu, S. Hu, et al., Polystyrene microplastics arrest skeletal growth in puberty through accelerating osteoblast senescence, Environ Pollut. 322 (2023) 121217. https://doi.org/10.1016/j.envpol.2023.121217.

[30] Y. Mori, A.K. Ajay, J.H. Chang, et al., KIM-1 mediates fatty acid uptake by renal tubular cells to promote progressive diabetic kidney disease, Cell Metab. 33 (2021) 1042-1061.e1047. https://doi.org/10.1016/j.cmet.2021.04.004.

[31] T. Wu, W. Zhu, R. Duan, et al., Magnetic vagus nerve stimulation ameliorates contrast-induced acute kidney injury by circulating plasma exosomal miR-365-3p, Journal of Nanobiotechnology. 22 (2024) https://doi.org/10.1186/s12951-024-02928-0.

[32] L. Yao, X. Liang, Y. Liu, et al., Non-steroidal mineralocorticoid receptor antagonist finerenone ameliorates mitochondrial dysfunction via PI3K/Akt/eNOS signaling pathway in diabetic tubulopathy, Redox Biol. 68 (2023) 102946. https://doi.org/10.1016/j.redox.2023.102946.

[33] K. Kapetanos, D. Asimakopoulos, N. Christodoulou, et al., Chronological Age Affects MSC Senescence In Vitro-A Systematic Review, Int J Mol Sci. 22 (2021) https://doi.org/10.3390/ijms22157945.

[34] J.M. Johnson, A.D. Peterlin, E. Balderas, et al., Mitochondrial phosphatidylethanolamine modulates UCP1 to promote brown adipose thermogenesis, Sci Adv. 9 (2023) eade7864. https://doi.org/10.1126/sciadv.ade7864.

[35] R. Ghosh, M. Malhotra, R.R. Sathe, et al., Biodegradable Polymer Theranostic Fluorescent Nanoprobe for Direct Visualization and Quantitative Determination of Antimicrobial Activity, Biomacromolecules. 21 (2020) 2896-2912. https://doi.org/10.1021/acs.biomac.0c00653.

[36] X. Wen, L. Tang, R. Zhong, et al., Role of Mitophagy in Regulating Intestinal Oxidative Damage, Antioxidants (Basel). 12 (2023) https://doi.org/10.3390/antiox12020480.

[37] P. Strzyz, Cell signalling: Signalling to cell cycle arrest, Nat Rev Mol Cell Biol. 17 (2016) 536. https://doi.org/10.1038/nrm.2016.108.

[38] Z. Cui, X. Zhao, F.K. Amevor, et al., Therapeutic application of quercetin in aging-related diseases: SIRT1 as a potential mechanism, Front Immunol. 13 (2022) 943321. https://doi.org/10.3389/fimmu.2022.943321.

[39]J.W. Hwang, H. Yao, S. Caito, et al., Redox regulation of SIRT1 in inflammation and cellular senescence, Free Radic Biol Med. 61 (2013) 95-110. https://doi.org/10.1016/j.freeradbiomed.2013.03.015.

[40] N.Y. Ngoi, A.Q. Liew, S.J.F. Chong, et al., The redox-senescence axis and its therapeutic targeting, Redox Biol. 45 (2021) 102032. https://doi.org/10.1016/j.redox.2021.102032.

[41] X. Deng, T. Zeng, J. Li, et al., Kidney-targeted triptolide-encapsulated mesoscale nanoparticles for high-efficiency treatment of kidney injury, Biomater Sci. 7 (2019) 5312-5323. https://doi.org/10.1039/c9bm01290g.

[42] P. Cohen, S. Kajimura, The cellular and functional complexity of thermogenic fat, Nat Rev Mol Cell Biol. 22 (2021) 393-409. https://doi.org/10.1038/s41580-021-00350-0.

[43] J.M. Oh, G. Kim, J. Jeong, et al., Compound K promotes thermogenic signature and mitochondrial biogenesis via the UCP1-SIRT3-PGC1α signaling pathway, Biomed Pharmacother. 183 (2025) 117838. https://doi.org/10.1016/j.biopha.2025.117838.

[44] K. Wang, Y. Du, P. Li, et al., Nanoplastics causes heart aging/myocardial cell senescence through the Ca(2+)/mtDNA/cGAS-STING signaling cascade, J Nanobiotechnology. 22 (2024) 96. https://doi.org/10.1186/s12951-024-02375-x.

[45] E. Bang, H. Hwangbo, H. Lee, et al., Exposure to polystyrene nanoplastics promotes premature cellular senescence through mitochondrial ROS production and dysfunction in pre-differentiated skeletal myoblasts, Toxicology. 510 (2025) 154002. https://doi.org/10.1016/j.tox.2024.154002.

[46] Y. Huang, X. Li, S. Xu, et al., Polyvinyl chloride nanoplastics suppress homology-directed repair and promote oxidative stress to induce esophageal epithelial cellular senescence and cGAS-STING-mediated inflammation, Free Radic Biol Med. 226 (2025) 288-301. https://doi.org/10.1016/j.freeradbiomed.2024.11.012.

[47] X. Li, Y. Huang, D. Zu, et al., PMMA nanoplastics induce gastric epithelial cellular senescence and cGAS-STING-mediated inflammation via ROS overproduction and NHEJ suppression, Ecotoxicol Environ Saf. 287 (2024) 117284. https://doi.org/10.1016/j.ecoenv.2024.117284.

[48] X. Guo, C. Cheng, L. Wang, et al., Polystyrene nanoplastics induce haematotoxicity with cell oxeiptosis and senescence involved in C57BL/6J mice, Environ Toxicol. 38 (2023) 2487-2498. https://doi.org/10.1002/tox.23886.

[49] G. Lu, S. Wei, Nanoplastics trigger the aging and inflammation of porcine kidney cells, Toxicology. 506 (2024) 153870. https://doi.org/10.1016/j.tox.2024.153870.

[50] J. Satriano, H. Mansoury, A. Deng, et al., Transition of kidney tubule cells to a senescent phenotype in early experimental diabetes, Am J Physiol Cell Physiol. 299 (2010) C374-380. https://doi.org/10.1152/ajpcell.00096.2010.

[51] J. Ma, W. Yang, F.M. Chen, et al., IRF8 and RUNX1 cooperatively regulate the senescence and damage of urine-derived renal progenitor cells by upregulating LINC01806, Biochem Pharmacol. 240 (2025) 117068. https://doi.org/10.1016/j.bcp.2025.117068.

[52] J. Chen, K.H. Chen, L.M. Wang, et al., Decoy receptor 2 mediates the apoptosis-resistant phenotype of senescent renal tubular cells and accelerates renal fibrosis in diabetic nephropathy, Cell Death Dis. 13 (2022) 522. https://doi.org/10.1038/s41419-022-04972-w.

[53] K. Chen, H. Dai, J. Yuan, et al., Optineurin-mediated mitophagy protects renal tubular epithelial cells against accelerated senescence in diabetic nephropathy, Cell Death Dis. 9 (2018) 105. https://doi.org/10.1038/s41419-017-0127-z.

[54] C. Jia, C. Ke-Hong, X. Fei, et al., Decoy receptor 2 mediation of the senescent phenotype of tubular cells by interacting with peroxiredoxin 1 presents a novel mechanism of renal fibrosis in diabetic nephropathy, Kidney Int. 98 (2020) 645-662. https://doi.org/10.1016/j.kint.2020.03.026.

[55] S. Kume, M. Kitada, K. Kanasaki, et al., Anti-aging molecule, Sirt1: a novel therapeutic target for diabetic nephropathy, Arch Pharm Res. 36 (2013) 230-236. https://doi.org/10.1007/s12272-013-0019-4.